Available online at www.sciencedirect.com
ScienceDirect
ELSEVIER
June 2016, 23(3): 94–100
www.sciencedirect.com/science/journal/10058885
The Journal of China Universities of Posts and Telecommunications
http://jcupt.bupt.edu.cn

Performance measurement of adaptive optics system based on Strehl ratio

Wang Liang[1,2], Chen Tao[1], Lin Xudong[1], Wei Peifeng[1,2], Liu Xinyue[1] (✉), Jia Jianlu[1]

1. Changchun Institute of Optics, Fine Mechanics and Physics, Chinese Academy of Sciences, Changchun 130033, China
2. University of Chinese Academy of Sciences, Beijing 100049, China

Abstract

In this article, a method for measuring the performance of adaptive optics (AO) systems is designed and validated by experiments. The Strehl ratio (SR) which is based on the target images is used to evaluate the performance quantitatively because it relates to the effect of AO correction directly. In the calculation of the SR, to avoid energy scaling in the diffraction-limited point spread function, an algorithm based on the integral of the optical transfer function (OTF) is proposed. Then, a 97-element AO system is established to validate this method, and a white-light fiber source is used as a point-like target. To simulate the practical conditions which influence the performance of the AO system, targets of different brightness are simulated in terms of different signal-to-noise ratios (SNRs) of the Shack-Hartmann (SH), and atmospheric turbulence is simulated in terms of the Fried's coherence length and the Greenwood's frequency. Finally, two experiments are conducted in which the SR of different simulated conditions are measured. The results of the experiments show that for a moderate SNR of SH the experimenting AO system is capable of closed-loop wavefront correction when the Fried's coherence length is larger than 5cm and the Greenwood's frequency is lower than 60 Hz. The results also show that the performance of AO is susceptible to the SNR of SH. The experiments validates the effectiveness of this method.

Keywords adaptive optics , performance measurement, Strehl ratio, turbulence simulator

1 Introduction

Recently, AO receives increasing attentions, not only owing to its traditional applications in the fields of astronomy and military equipments [1], but also owing to its fresh applications in laser communication [2], ophthalmology [3] and high-resolution microscopy [4]. Typically, an AO system is composed of a wavefront sensor (WFS), a wavefront corrector (WFC) and a control system [5]. When AO is working, the WFS measures the wavefront distortion in real time and the WFC counteracts this distortion accordingly. And then, the resolution of target images are improved after the AO correction. The most common-used WFS is SH and the common WFC includes deformable mirror (DM) [6] and liquid-crystal corrector [7–8].

The motivation of this article is the requirement of developing a method for assessing the performance of an experimental AO system. Through this method, the factors which affect the performance of AO system, such as the control strategies and calibration strategies can be researched. Also using this method, the wavefront processor (WFP) [9], an embedded system which can accelerate the process of wavefront control, can be tested.

The performance measurement of an AO system can be conducted on the telescope in which the AO system is integrated. Then the performance can be measured in terms of the residual wavefront aberrations, when the AO system is correcting the wavefront which originates from a star and is distorted by the real atmospheric turbulence. Similar measurements have been carried out by Liu et al who measure the performance of an AO system for free-space coherent laser communication [10], by Roberts et al who characterize the AO system of the advanced electro-optical system (AEOS) telescope [11], and by Dam et al who

Received date: 10-12-2015
Corresponding author: Liu Xinyue, E-mail: sirliuxy@hotmail.com
DOI: 10.1016/S1005-8885(16)60038-9

characterize the AO system of the W. M. Keck Observatory [12]. However, this configuration is only suitable for a finishing AO system and is not appropriate for a laboratorial AO system which is being optimized. In this paper, the performance measurement will be implemented on an optical bench where an atmospheric turbulence simulator is configured.

For the purpose of performance measurement, an evaluation index is required to measure the system performance quantitatively in different testing environments simulated in the laboratory. SR is a common-used metric for the performance measurement of AO systems [13–14]. In Ref. [11], Robert et al characterized the AEOS AO system using the SR which is calculated from the images of stars. SR outperforms other evaluation indices based on SH such as root of mean square (RMS) of residual aberrations because SR can be measured based on the AO-corrected target images directly. Also, SR may directly relate to certain system parameters for some applications of AO. For example, when AO is applied to compensate aberrations in the free space optical communications, SR can be used to approximate fiber-coupling efficiency [15–17]. Although SR has been used to estimate the correction accuracy of AO system [18–19], essentially, the calculation of SR is based on SH in these papers, because it is calculated by residual aberrations measured by SH. As a result, SR calculated by this method are susceptible to non-common path aberrations between SH and imaging camera [5,20]; also, it can be influenced by truncation error caused by finite Zernike polynomials which is use to fit residual aberrations measured by SH. Therefore, SR is calculated according to the AO-corrected target images. For the calculation of the SR, to avoid energy scaling in the diffraction-limited point spread function, an algorithm based on the integral of the OTF is proposed.

The rest of this article is organized as follows. A method for calculating SR based on target images is developed in Sect. 2. The experiment system for AO performance measurement is established in Sect. 3. The method of simulating practical environments are introduced and how to measure testing parameters are discussed in Sect. 4. The experiment results of performance measurement are shown and discussed in Sect. 5. Sect. 6 summarizes this article.

2 Method for calculating SR

The SR R_{SR} of an optics system is defined as the ratio of the peak intensity of a measured point spread function (PSF) to the peak intensity of a diffraction-limited PSF [13],

$$R_{\mathrm{SR}}=\frac{\max\limits_{\boldsymbol{x}}\left\{I_{\mathrm{m}}(\boldsymbol{x})\right\}}{\max\limits_{\boldsymbol{x}}\left\{I_{\mathrm{dl}}(\boldsymbol{x})\right\}} \tag{1}$$

where the vector $\boldsymbol{x}$ denotes coordinates in the imaging plane, $I_{\mathrm{m}}(\boldsymbol{x})$ denotes the measured PSF and $I_{\mathrm{dl}}(\boldsymbol{x})$ denotes the diffraction-limit PSF. The measured PSF can be obtained from the imaging camera when a white-light fiber source is adopted as a point source. The diffraction-limit PSF can be obtained by using an Inverse Fourier transform of an aberration-free generalized pupil function $P(\boldsymbol{u})$ [21],

$$I_{\mathrm{dl}}(\boldsymbol{x})=\left|\mathcal{F}^{-1}\left\{P(\boldsymbol{u})\right\}\right|^2 \tag{2}$$

where the vector $\boldsymbol{u}$ denotes coordinates in the pupil plane, and the functor $\mathcal{F}^{-1}$ refers to the inverse Fourier transform. The function $P(\boldsymbol{u})$ is a binary mask which is defined as follows [21],

$$P(\boldsymbol{u})=\begin{cases}1; & \|\boldsymbol{u}\|_2\leqslant r_{\mathrm{p}}\\ 0; & \|\boldsymbol{u}\|_2> r_{\mathrm{p}}\end{cases} \tag{3}$$

where r_{p} denotes the radius of the pupil. Easy to find from Eqs. (2), (3) that an energy mismatch exists between the measured PSF and the diffraction-limit PSF, therefore, the latter should be scaled to match the former's energy. Lewis et al. proposed an equation for calculating SR in spatial frequency domain in Ref. [13],

$$R_{\mathrm{SR}}=\frac{\int\limits_{\|\boldsymbol{f}\|_2\leqslant f_{\mathrm{c}}}\mathcal{H}_{\mathrm{m}}(\boldsymbol{f})\,\mathrm{d}\boldsymbol{f}}{\int\limits_{\|\boldsymbol{f}\|_2\leqslant f_{\mathrm{c}}}\mathcal{H}_{\mathrm{dl}}(\boldsymbol{f})\,\mathrm{d}\boldsymbol{f}} \tag{4}$$

where the vector $\boldsymbol{f}$ denotes coordinates in spatial frequency domain, f_{c} denotes the cut-off frequency of the optical system, $\mathcal{H}_{\mathrm{m}}(\boldsymbol{f})$ and $\mathcal{H}_{\mathrm{dl}}(\boldsymbol{f})$ denote the OTF of AO-corrected system and diffraction- limit system, respectively, which are defined as follows

$$\mathcal{H}_{\mathrm{m}}(\boldsymbol{f})=\frac{\mathcal{F}\left\{I_{\mathrm{m}}(\boldsymbol{x})\right\}}{\int I_{\mathrm{m}}(\boldsymbol{x})\,\mathrm{d}\boldsymbol{x}} \tag{5}$$

$$\mathcal{H}_{\mathrm{dl}}(\boldsymbol{f})=\frac{\mathcal{F}\left\{I_{\mathrm{dl}}(\boldsymbol{x})\right\}}{\int I_{\mathrm{dl}}(\boldsymbol{x})\,\mathrm{d}\boldsymbol{x}} \tag{6}$$

where the functor $\mathcal{F}$ refers to the Fourier transform. Seen from Eqs. (5), (6), energy normalization is done when calculating the OTF; therefore, the energy match is

unnecessary when using Eq. (4) to obtain SR.

3 Experiment setup for AO performance measurement

The layout of optics for AO performance measurement is shown in Fig. 1. The light source is a white-light source (The wavelengths of the light distribute from 400 nm to 2 400 nm.) comprising a single fiber and the diameter of the fiber is 25 μm. Because the diameter of the fiber is much smaller than the focal length of the lens L1 (3 000 mm), this light source can be considered as a point-like light source approximately. The turbulence simulator is a phase plate which is produced by Lexitek Co., and its coherence length is 0.6 mm (at the wavelength of 632.8 nm). The phase plate simulates atmospheric turbulence of a certain Greenwood's frequency when it is rotating at a constant angular velocity. As will be discussed in Sect. 4, when the angular velocity of the phase plate and the distance towards light source of the phase plate are changed, two atmospheric parameters, i.e. the Fried's coherence length and the Greenwood's frequency are adjusted respectively. In other words, all kinds of atmospheric turbulence can be simulated using this method. The tip/tilt mirror (TM) is a fast steering mirror which can correct aberrations of low orders, i.e. the tip and tilt. The DM is a 97-element continuous-surface DM. The RMS and peak to valley (PV) of this DM is 0.043 wave and 0.521 wave, respectively, when it is flattened as the method proposed in Ref. [22], using a Zygo interferometer. The SH has 97 subapertures, as is shown in Fig. 2. Both the DM and the SH are developed by Electro-Optical Detection (EOD) Department, Changchun Institute of Optics, Fine Mechanics and Physics (CIOMP), Chinese Academy of Sciences. As is designed and simulated by Zemax, the entrance pupil is the DM, so the extent of the optical wavefront is limited by the DM. In Fig. 1, the real lines represent the rays emitting from the fiber source, and the dashed lines represent the practical rays which pass the entrance pupil of the AO system.

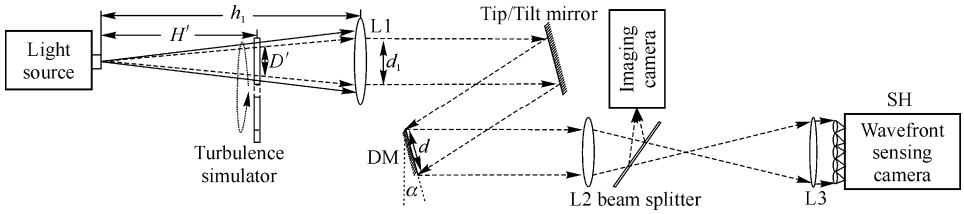

Fig. 1 Layout of optics for AO performance measurement

4 Testing environment simulation

4.1 The brightness of target

The brightness of different targets for AO correction is often different, which causes different SNRs in SH. Because the average SNR of SH is much easier to measure than the brightness of targets, this SNR is adopted to represent different brightness. To simulate different brightness, an adjustable light source is chosen.

The SNR of each subaperture is calculated as Ref. [23]. The SNR of the i-th subaperture is as follows,

$$R_{\mathrm{SNR},i}=\frac{\sum_{x\in A_i} I(\boldsymbol{x})}{\sum_{x\in A_i} -\mu_{\mathrm{B},i}}}{\sigma_{\mathrm{B},i}} \tag{7}$$

where $\mu_{\mathrm{B},i}$ and $\sigma_{\mathrm{B},i}$ are the average and the standard variation of the background in the i-th subaperture, respectively. The background can be obtained from the imaging camera when the light source is tuned off. $I(\boldsymbol{x})$ is a image obtained by SH with the light source on, and A_i refers to the spot area of the i-th subaperture. To be simplified, the spot area is set to be a 4 pixel by 4 pixel area sharing the same center with the spot. Then, the average SNR can be obtained by calculating the average of all the subapertures. Several SH images of different average SNR are illustrated in Fig. 2, after a threshold process as in Ref. [24]. In Fig. 2, the number printed in each subaperture is the SNR of each subaperture, respectively.

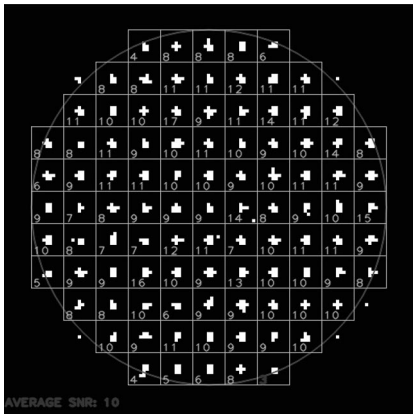

(a) Average SNR is 10

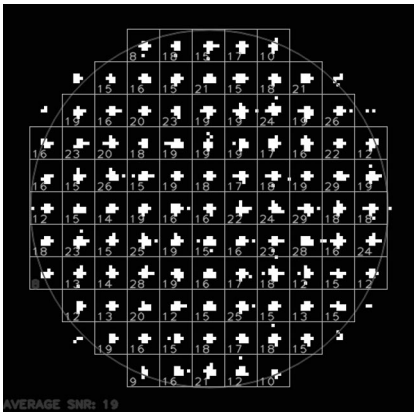

(b) Average SNR is 19

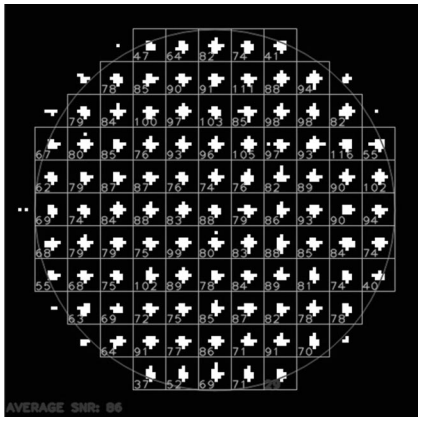

(c) Average SNR is 86

Fig. 2 Illustrating images of SH with different average SNR

4.2 The Fried's coherence length

The Fried's coherence length r_0 is a common-used descriptor to represent the strength of atmospheric turbulence. As is shown in Ref. [25], the Fried's coherence length can be calculated by

$$r_0 = \frac{r_0' D}{D'} \tag{8}$$

where r_0' denotes the coherence length of the phase plate (0.6 mm@632.8 nm). D denotes the diameter of the pupil of the telescope where the AO system is used (It is supposed D is 1.2 m in the simulation.). D' denotes the effective diameter of the beam at the phase plate, because the extent of the optical wavefront is limited by the entrance pupil, i.e. the DM. D' can be calculated by

$$\frac{D'}{d_1} = \frac{H'}{h_1} \tag{9}$$

As is shown in Fig. 1, h_1 denotes the distance between the lens L1 and the fiber source, and H' denotes the distance between the phase plate and the fiber source. Here, d_1 denotes the effective diameter of the beam at the lens L1 which can be obtained by

$$d_1 = d\cos\alpha \tag{10}$$

where d denotes the diameter of the DM and α denotes the angle as is shown in Fig. 1. Then, different r_0 can be obtained by adjusting the distance between the light source and the phase plate. The Fried's coherence length in this paper corresponds to a wavelength of 632.8 nm, and the Fried's coherence length at other wavelength can be calculated similarly, using the coherence length of the phase plate at the corresponding wavelength.

4.3 The Greenwood's frequency

The Greenwood's frequency f_G is always used as a measure of the rate at which the turbulence changes with time. With different angular velocities of the phase plate, different Greenwood's frequencies can be simulated. According to Ref. [16], the Greenwood's frequency can be obtained by

$$f_G = 0.427\frac{V}{r_0'} \tag{11}$$

where V denotes the linear velocity of the phase plate at the center of the optical beam.

5 Results of AO performance measurement

Two experiments are carried out to measure the performance of the AO system as shown in Fig. 1. First, AO performance are measured for different r_0, when the SNR of the SH is fixed at a moderate value. Second, performance measurement is conducted for different SNR

of the SH, when r_0 is 11cm.

Before the experiments, the AO system are calibrated using the method of controlling gradient directly (CGD) [27] in order to obtain an influence matrix. The influence matrix represent the responses of AO system in terms of the spot shifts of the SH, when the voltage on each actuator of the DM is increased by a unit quantity one by one. Then, the reconstruction matrix can be obtained by calculating the pseudo-inverse of the influence matrix, using a singular value decomposition (SVD) method. With the reconstruction matrix, the voltage on each actuator can be evaluated for wavefront correction. A proportional-integral (PI) control strategy is adopted for a closed-loop wavefront correction. The frequency of wavefront correction is 500 Hz.

5.1 AO performance measurement for different r_0

In the first experiment, the SNR of the SH is fixed. So in the beginning, the brightness of the light source is adjusted until the SNR of the SH is about 30. Then, four kinds of r_0 are simulated, i.e. 5 cm, 7 cm, 9 cm and 11 cm. For each r_0, ten Greenwood's frequencies are simulated, from 10 Hz to 100 Hz with an increment of 10 Hz. For each condition, AO correction is conducted, and 50 images are recorded by the imaging camera to calculate the average SR. The result of this experiment is shown in Fig. 3. The images of targets before and after AO-correction, which are obtained from the imaging camera, are shown in Fig. 4.

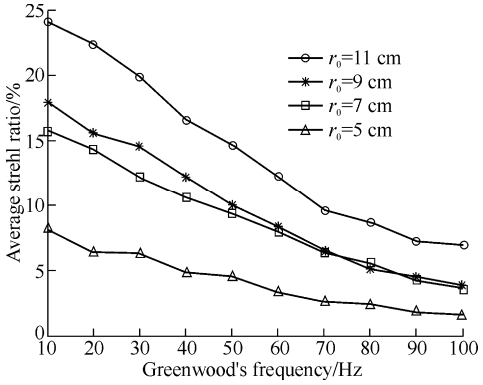

Fig. 3 Measured average SRs versus different Greenwood's frequencies for different Fried's coherence lengths (The average SNR of SH is 30)

Seen from Fig. 3, it can be found that for the cases when r_0 is 7 cm, 9 cm and 11 cm, the AO correction is good when f_G is lower than 60 Hz. It can be also found that AO system works poorly when r_0 is 5 cm. Here, a criterion that SR is over 10% is adopted to decide whether the AO correction is good or not. Also, it can be noted that SR decreases as the Fried's coherence length is reduced, when the Greenwood's frequency is fixed. This can be explained by a fact that the fitting error of the closed-loop AO system increases as the Fried's coherence length is reduced, and consequently, the SR decreases.

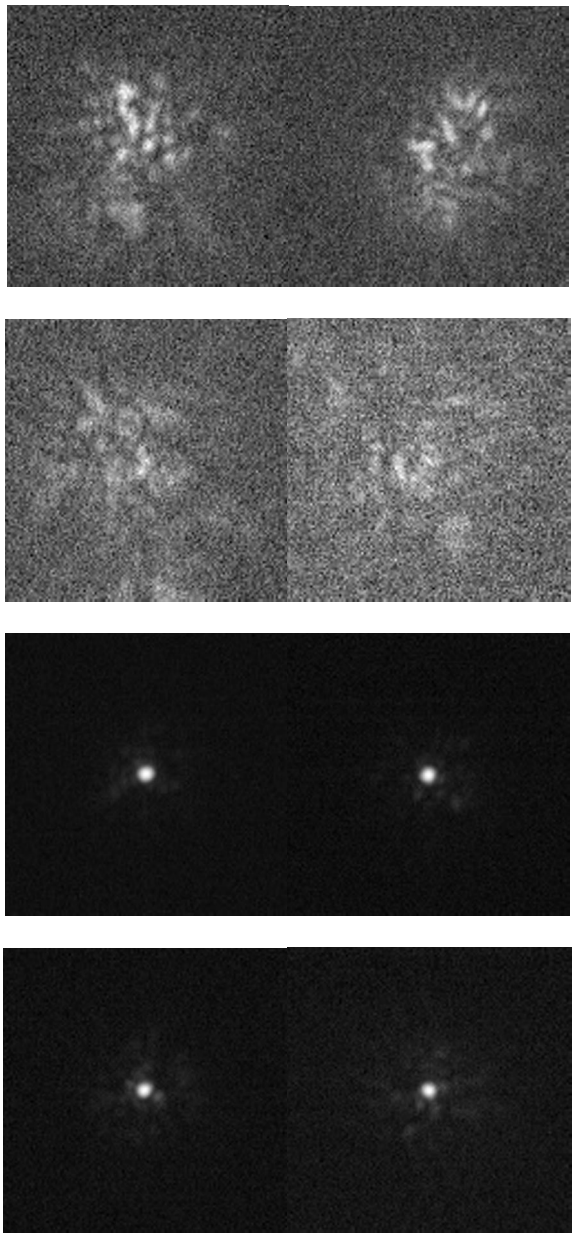

Fig. 4 Images of the target before AO correction (top four images) and after AO correction (bottom four images) for different r_0 (The images are obtained when the average SNR of the SH is 30 and the Greenwood's frequency is 30 Hz. The images from top left to bottom right correspond to the Fried's lengths of 11 cm, 9 cm, 7 cm and 5 cm, respectively)

5.2 AO performance measurement for different average SNR of SH

In the second experiment, AO performance of different average SNR of SH is measured when r_0 is 11 cm. By adjusting the brightness of the light source, the average SNR of SH are set to four values, i.e. 10, 20, 40 and 100. And for each SNR, similar to section 5.1, the turbulence is simulated at ten Greenwood's frequencies from 10 Hz to 100 Hz with an increment of 10 Hz, and SR is measured during AO correction. The result of this experiment is shown in Fig. 5.

It can be found that the decrease in average SNR of the SH lowers AO performance considerably, when the average SNR is reduced from 40 to 20, and from 20 to 10. This is resulted from the decrease in the accuracy of the centroid extraction of SH. However, it can be noted that a significant decrease in the average SNR of the SH from 100 to 40 results in only a slight decrease in SR on the whole. Furthermore, it can be observed that SNR-40 SR surpasses SNR-100 SR a little when the Greenwood's frequency is 80 Hz. It can be concluded that increasing the average SNR of the SH will not have very obvious effect on the performance of a closed-loop AO system when the average SNR of the SH is high enough. This can be explained by the fact that the noise error of a closed-loop AO system is not in a dominant position when the average SNR of the SH is high enough. And at that time, efforts should be made on suppressing other errors which may be in a dominant position such as the calibrating error, the fitting error and the bandwidth error [1], so as to improve the system performance.

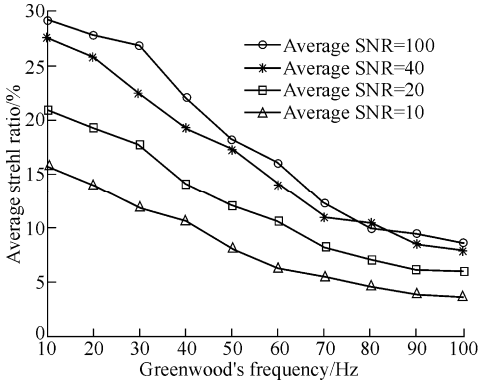

Fig. 5 Measured average SRs versus different Greenwood's frequencies for different average SNR of SH(r_0 =11 cm)

6 Conclusions

This study mainly designs a SR-based method for measuring the performance of AO systems and validates its effectiveness by experiments. In order to simulate different practical conditions which affect the performance of the AO system, targets of different brightness are simulated, and different atmospheric turbulence is simulated in terms of different Fried's coherence lengths and different Greenwood's frequencies. Two experiments are conducted on a 97-element AO system to measure the SR under different simulated conditions. The results show that the experimenting AO system is capable of closed-loop wavefront correction when r_0 is larger than 5 cm and f_G is lower than 60 Hz for a moderate SNR of SH (about 30). The results also show that the performance of AO is susceptible to the SNR of SH. The experiments validate the effectiveness of this method. This method is feasible for laboratorial performance measurement of closed-loop AO systems, which can be applied to the fields such as astronomical telescopes and laser communications.

Acknowledgements

This work was supported by the National High Technology Research and Development Program of China (2014AAXXX1003X).

References

1. Hardy J W. Adaptive optics for astronomical telescopes. New York, NY, USA: Oxford University Press: 1998: 3–24
2. Huang J, Zhang P, Deng K, et al. Boundary parameters of adaptive optical system in satellite to ground coherent laser communication system. Optics and Precision Engineering, 2014, 22(5): 1204–1211 (in Chinese)
3. Liang J, Williams D R, Miller D T. Supernormal vision and high-resolution retinal imaging through adaptive optics. Journal of the Optical Society of America, 1997, 14(11): 2884–2892
4. Booth M J. Adaptive optical microscopy: The ongoing quest for a perfect image. Light: Science & Applications, 2014, 3:e165.
5. Wang L, Chen T, Liu X Y, et al. Compensation of the non-common path aberrations in an adaptive optics system with a wavefront processor. Acta Photonica Sinica, 2015, 44(5): 0511001 (in Chinese)
6. Lin X D, Liu X Y, Wang J L, et al. Progress of the continuous surface deformable mirror based on piezo-ceramic actuator. Laser & Optoelectronics Progress, 2014, 51(9): 090003 (in Chinese)
7. Xuan L, Li D Y, Liu Y. Prospect of liquid crystal adaptive optics in astronomy application. Chinese Journal of Liquid Crystals and Displays, 2015, 30(1): 1–9 (in Chinese)
8. Mu Q Q, Cao Z L, Peng Z H, et al. Modal interaction matrix measurement for liquid-crystal corrector: Precision evaluation. Optics Express, 2009, 17(11): 9330–9336
9. Yang H F, Xia Y X, Zhang H T, et al. Efficient and low-latency pixel data transmission module for adaptive optics wavefront processor based on field-programmable gate array. Optical Engineering, 2015, 54(6): 063106

10. Liu C, Chen S Q, Liao Z, et al. Correction of atmospheric turbulence by adaptive optics in waveband of free-space coherent laser communication. Optics and Precision Engineering, 2014, 22(10): 2605−2610 (in Chinese)
11. Roberts L C Jr, Neyman C R. Characterization of the AEOS adaptive optics system. The Publications of the Astronomical Society of the Pacific, 2002, 114(801):1260−1266
12. van Dam M A, Bouchez A H, Le Mignant D, et al. The W. M. Keck observatory laser guide star adaptive optics system: performance characterization. The Publications of the Astronomical Society of the Pacific, 2006, 118: 310−318
13. Roberts J C Jr, Perrin M D, Marchis F, et al. Is that really your Strehl ratio. Proceedings of SPIE, 2004, 5490: 504−515
14. Guo Y M, Rao C H, Bao H, et al. Multichannel-Hadamard calibration of high-order adaptive optics systems. Optics Express, 2014, 22(11): 13792−13803
15. Weyrauch T, Vorontsov M A. Atmospheric compensation with a speckle beacon in strong scintillation conditions: Directed energy and laser communication applications. Applied Optics, 2005, 4(30): 6388−6401
16. Han L Q, Wang Z B. Fiber coupling efficiency and Strehl ratio for space optical communication based on adaptive optics correction. Infrared and Laser Engineering, 2013, 42(1):125−129 (in Chinese)
17. Xiong Z, Ai Y, Shan X, et al. Fiber coupling efficiency and compensation analysis for free space optical communication. Infrared and Laser Engineering, 2013, 42(9): 2510−2514(in Chinese),
18. Bai F Z, Rao C H. Effect of pinhole diameter on correction accuracy of closed-loop adaptive optics system using self-referencing interferometer wavefront sensor. Acta Physica Sinica, 2010, 59(11): 8280−8286 (in Chinese)
19. Mu J, Rao C H, Li M, et al. The embedded processing platform design based on FPGA and DSP of an adaptive optics system on-line performance evaluation. Opto-Electronic Engineering, 2012, 39(6): 34−40 (in Chinese)
20. Sauvage J F, Fusco T, Rousset G, et al. Calibration and precompensation of noncommon path aberrations for extreme adaptive optics. Journal of the Optical Society of America, 2007, 24(8): 2334−2346
21. Goodman J W. Introduction to Fourier optics. 2nd ed. New York, NY, USA: McGraw-Hill, 1996: 126−150
22. Sivaramakrishnan A, Oppenheimer B R. Deformable mirror calibration for adaptive optics systems. Proceedings of SPIE, 1998, 3353: 910−916
23. Ren J F, Rao C H, Li M Q. An adaptive threshold selection method for hartmann-shack wavefront sensor. Opto-Electronic Engineering, 2002, 29(1):1−5 (in Chinese)
24. Ma X Y, Rao C H, Zheng H Q. Error analysis of CCD-based point source centroid computation under the background light.Optics Express, 2009, 17(10): 8525−8541
25. Wei P F, Lu Z W, Liu X Y, et al. Performance analysis of adaptive optical system for spatial objectives. Acta Photonica Sinica, 2015, 44(7): 0701001 (in Chinese)
26. Wei P F, Liu X Y, Lin X D, et al. Temporal simulation of atmospheric turbulence during adaptive optics system testing. Chinese Optics, 2013, 6(3): 371−377 (in Chinese)
27. Jiang W, Li H. Hartmann-Shack wavefront sensing and wavefront control algorithm. Proceedings of SPIE, 1990, 1271: 82−93

(Editor: Lu Junqiang)